Closed-loop Control of Functional Neuromuscular Stimulation

NIH Neuroprosthesis Program Contract Number N01-NS-6-2338
Quarterly Progress Report #8
January 1, 1998 to March 31, 1998

Investigators:
Patrick E. Crago, Ph.D.
Clayton L. Van Doren, Ph.D.
Warren M. Grill, Ph.D.
Michael W. Keith, M.D.
Kevin L. Kilgore, Ph.D.
Joseph M. Mansour, Ph.D.
Wendy M. Murray, PhD.
P. Hunter Peckham, Ph.D.
David L. Wilson, Ph.D.

Departments of
Biomedical Engineering,
Mechanical and Aerospace Engineering,
and Orthopaedics
Case Western Reserve University
and MetroHealth Medical Center

THIS QPR IS BEING SENT TO YOU BEFORE IT HAS BEEN REVIEWED BY THE STAFF OF THE NEURAL PROSTHESIS PROGRAM.

1. SYNTHESIS OF UPPER EXTREMITY FUNCTION

The overall goals of this project are (1) to measure the biomechanical properties of the neuroprosthesis user's upper extremity and incorporate those measurements into a complete model with robust predictive capability, and (2) to use the predictions of the model to improve the grasp output of the hand neuroprosthesis for individual users.

1. a. BIOMECHANICAL MODELING: PARAMETERIZATION AND VALIDATION

Purpose

In this section of the contract, we will develop methods for obtaining biomechanical data from individual persons. Individualized data will form the basis for model-assisted implementation of upper extremity FNS. Using individualized biomechanical models, specific treatment procedures will be evaluated for individuals The person-specific parameters of interest are tendon moment arms and lines of action, passive moments, and maximum active joint moments. Passive moments will be decomposed into components arising from stiffness inherent to a joint and from passive stretching of muscle-tendon units that cross one or more joints.

Report of progress

1. a. i. MOMENT ARMS VIA MAGNETIC RESONANCE IMAGING

Abstract

In this quarter, we completed a manuscript describing the estimation of tendon moment arms at the MP joint of the long finger. We have also begun to apply these techniques to analyze the biomechanics of the extensor carpi ulnaris to extensor carpi radialis brevis tendon transfer.

Progress Report

We have completed a manuscript describing our work to date on the MP joint of the long finger. This manuscript will be submitted for review in June. The title, authors and abstract follow.

Title: Estimation of Tendon Moment Arms from 3D MRI Images

Authors: David L. Wilson, Qian Zhu, Jeffrey L. Duerk, Joseph M. Mansour, Kevin Kilgore, and Patrick E. Crago

Abstract: New three-dimensional (3D) magnetic resonance imaging (MRI) methods were created and used to measure the tendon moment arm of the flexor digitorum profundus at the third metacarpophalangeal (MCP) joint. Using an open magnet MRI system and a hand holder, a series of static images were acquired at four joint angles and analyzed using specially created computer programs. Three methods were evaluated: (1) a 3D tendon excursion method that extended the method of Landsmeer, (2) a 3D geometric method whereby the moment arm was the perpendicular distance between the joint axis of rotation and the tendon path, and (3) a 2D geometric method whereby single image slices were analyzed. Repeating the imaging and measurement process, the 3D tendon excursion method was more reproducible (6% variation) than the 3D geometric method (12%), and both were much more reproducible than the 2D geometric method (27%). By having three operators analyze a single set of image data, we found that the precision of the 3D tendon excursion method was much less affected by segmentation error than the 3D geometric method. As a result of tendon bowstringing and displacement of the joint center of rotation toward the dorsal side of the hand, moment arm increased as a function of joint flexion by as much as 60%. Because of the dependence on flexion and variation between subjects, we recommend patient-specific measurements for target applications in functional neuromuscular stimulation interventions and tendon transfer surgery.

We have also begun the steps necessary to apply the biomechanical imaging techniques to analyze the biomechanics of the ECU to ECRB tendon transfer procedure. We documented and organized the programs used to analyze tendon moment arms. A new graduate student has learned the image acquisition and analysis steps, and we have acquired one set of images of the wrist to practice the techniques. We are

currently designing the test protocol, including the angles to be set. In order to analyze the transfer, we will analyze the moment arm of the ECU in radial/ulnar deviation, and the ECRB in flexion/extension.

Plans for next quarter

We will continue the application of the biomechanical imaging analysis of tendon moment arms at the wrist.

1.a.ii. PASSIVE AND ACTIVE MOMENTS

Abstract

During the past quarter, we began working on the design of a new device for measuring passive moments of the metacarpophalangeal and proximal interphalangeal joints of the fingers. The primary feature of this new design is that it is capable of maintaining a fixed joint angle without the use of splints. This is accomplished by applying the appropriate forces and moments to the finger tip. During this quarter, the mechanical principles of the design were analyzed. Using a detailed proposed experimental protocol, we were able to estimate the expected errors in measurement using known error values for the individual force and position transducers. The results indicate that joint moments can be measured to within +/- 1 N-cm, which is comparable to the accuracy of our current passive moment device.

Purpose

The purpose of this project is to characterize the passive properties of normal and paralyzed hands. This information will be used to determine methods of improving hand grasp and hand posture in FES systems.

Report of Progress

The information obtained regarding the passive moments at the index metacarpophalangeal (MP) joint as a function of wrist angle have been reported in previous progress reports. This information has allowed us to develop a model describing the contributions of the extrinsic and intrinsic tissues to the total passive moment. With this model we were able to determine that there are not large differences in many of the passive properties of the paralyzed hand vs. the normal hand at the MP joint of the finger. We did find that in some paralyzed individuals the flexor tendons produced a much greater portion of the passive moment when compared to the average normal. This probably indicates a shortened flexor muscle/tendon unit. We would like to proceed with this investigation by attempting to separate the contribution of the flexor digitorum superficialis (FDS) from the contribution of the flexor digitorum profundus (FDP). We would also like to include an analysis of the passive properties at the proximal interphalangeal (PIP) and distal interphalangeal (DIP) joints because we anticipate that their properties will be quite different between paralyzed and normal hands.

In order to analyze the more distal joints of the finger, it is necessary to modify the apparatus that we have successfully used with the MP joint. We have found that it is extremely difficult to construct a splint that can hold the MP joint in place while the PIP joint is rotated. It is even more difficult to hold the MP and PIP joints while the DIP joint is rotated. Multiple splints must be constructed if different MP and PIP angles are to be tested. Even if satisfactory splints could be built, they would have to be custom made to fit each subject. Because of these limitations, we have looked into a splint-free method of "fixing" the joints in place. During this quarter, we have developed an initial design and analyzed the expected output mathematically to determine if the accuracy of the device will be sufficient for the measurements necessary for this project.

Design Features

The development of a new device to measure passive moment was motivated primarily by three features:

1) to be able to independently maintain a constant position of the MP joint while rotating the PIP joint, and vice versa.

2) to be able to independently position and move all four fingers at the same time
3) minimize the splinting applied to the fingers.

In addition, our experience in making passive moment measurements has led us to believe that it is necessary for the device to perform these operations automatically under computer control. It is too difficult and too time consuming for a human operator to have to manually adjust the angles of each finger between trials.

Description of Passive Moment Device

The basic premise of the splintless apparatus for the measurement of passive moments is that the MP and PIP joints can be made to move independently by applying the appropriate forces to the tip of the finger. The forces would be applied through a splint on the tip of the finger (an adjustable thimble), as shown in Figure 1.a.ii.1. If the forces at the tip are known, and the joint angles are known, it should then be possible to calculate the joint moments. The forces would be applied by positioning the finger using a X-Y translating frame with a torque motor to apply torque to the finger tip. It should be possible to cascade four similar units so that all four fingers can be moved independently.

Mechanical Principles of Passive Moment Device

A free body diagram of the finger attached to the device is shown in Figure 1.a.ii.1. In order for the device to operate properly, it must be possible to independently change Mpip while keeping Mmp constant, and vice versa, by changing the two forces and one moment applied at the tip of the finger. The moment is applied using a torque motor and the forces are applied using an X-Y translating frame.

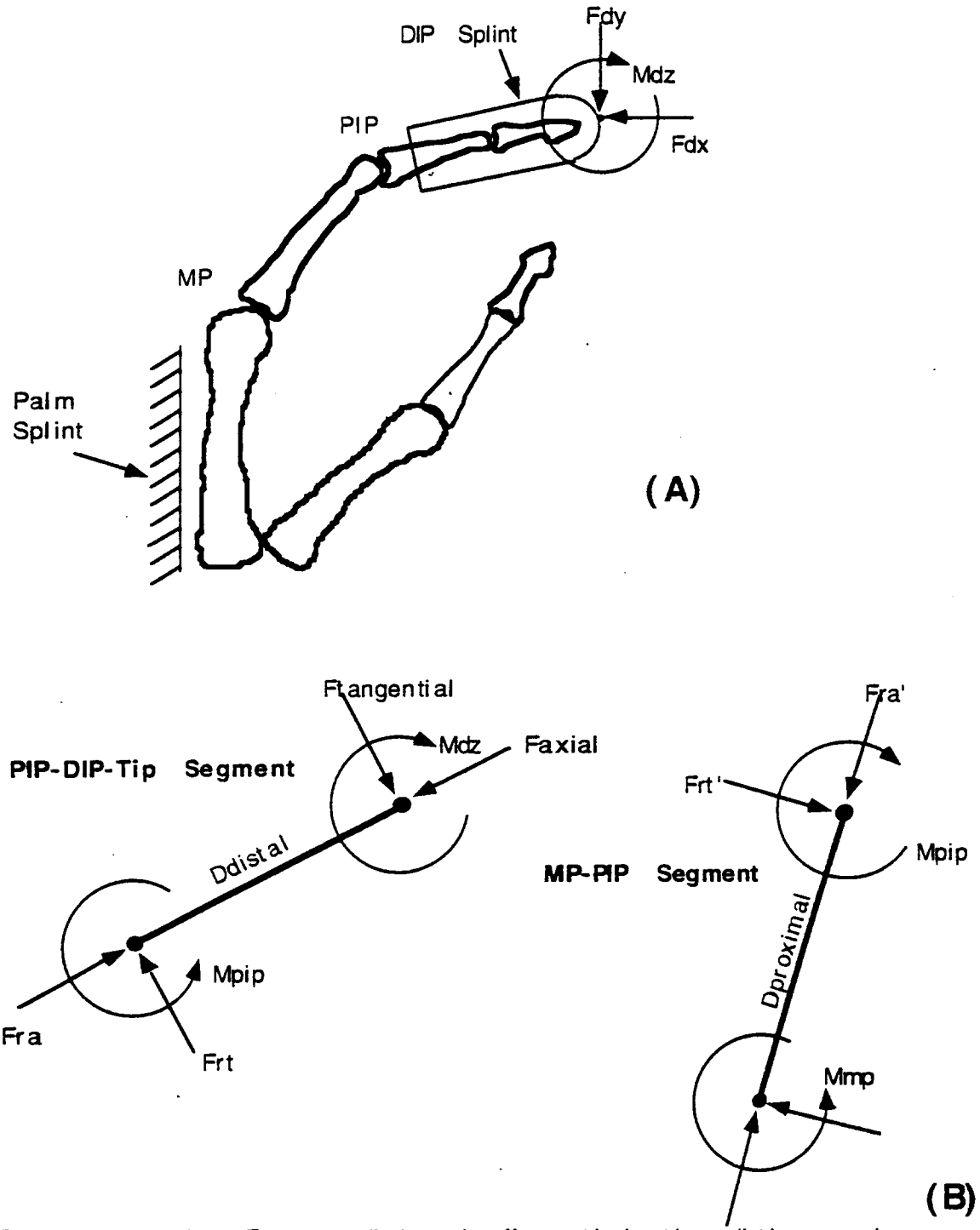

Figure 1.a.ii.1. (A) Forces applied to the finger tip by the splintless passive moment device. (B) Free body diagram of the distal segment (left) and the proximal segment (right). The device must apply the appropriate forces on the finger tip in order to independently control Mpip and Mmp.

For the distal segment, the moment about the PIP joint can be calculated as follows:

$$Mpip = Mdz + Ftang \bullet Ddistal$$

where:
Mpip = applied moment about PIP joint
Mdz = moment applied by the transducer on the tip of the finger
Ftang = tangential force applied to the tip of the finger
Ddistal = distance between the force application and the center of rotation of the PIP joint

also,

$$Mmp = Mpip + Frt' \bullet Dproximal$$

where:
Mmp = applied moment about the MP joint
Frt' = tangential reaction force at PIP joint (note that the coordinate system is rotated from the system defined for the distal segment. A simple transformation can be defined between the reaction forces.)
Dproximal = distance between the center of rotation of the PIP joint and the center of rotation of the MP joint.

It can be seen that the moment at the PIP joint is affected by both the tangential force and the moment applied by the device. If Ftang is increased by an amount ΔF, and Mdz is decreased by an amount equal to $\Delta F \bullet$Ddistal, then Mpip remains constant. However the new Mmp (Mmp*) is now:

$$Mmp^* = Mpip + Frt'^* \bullet Dproximal,$$

where Frt'* is either larger or smaller, depending on the size and direction of ΔF. Therefore, Mmp will be changed while Mpip remains constant. It can be shown that the same procedure can be followed to allow Mmp to remain constant while Mpip is changed. This analysis establishes the basic feasibility of the splintless passive device.

Predicted Error Analysis of Passive Moment Device

It is important to verify mathematically that it is possible to use this device to make accurate measurements. We identified two potential sources of considerable measurement error with this design. In this section, we describe those two sources of error, describe our mathematical method for evaluating the anticipated error, and report on the expected error values that were calculated.

The two major sources of error in this device are: 1) joint centers of rotation must be estimated and 2) joint angles must be accurately known. We believe that we have been able to develop techniques which will reduce both of these sources of error so that accurate measurements of the passive joint properties can be obtained.

First, in order to calculate joint moments, the moment arms must be known. In order to know the moment arm distances, the center of rotation of the PIP and MP joints must be known. Any estimate of the moment arm is subject to error, and the error is compounded when it is propagated through multiple joint segments. A simple visual estimation of the center of rotation, with a likely error of around +/- 5mm, can produce a direct error of 20% in the calculated joint moment values (given a segment length of 5cm). In addition, the mechanical analysis of the device demonstrated that it is necessary to have accurate

measurements of the joint center of rotation so that the correct forces and moments can be applied to the finger tip in order to position the finger properly.

One possible solution to this problem is to allow the apparatus itself to determine where the joint centers of rotation are located. This can be done using the kinematics of the joint as the device moves the finger through space. If the joint angles can be known during finger movement, the manner in which they move relative to each other and to the hand should indicate where the center of rotation is for each joint, assuming that the center of rotation remains constant. This solution, however, leads to a second potential source for error, which is the measurement of the angles of the MP and PIP joints. For example, in order to get moment arm errors below 3%, we determined that it was necessary to know the joint angles within +/- 0.5 degrees (2 STD) and the positions within +/- 0.1 mm (2 STD). Moment arm errors translate directly into errors in the joint moment estimation. Any errors in the force measurement at the tip of the finger will just compound the problem. In addition, the need to apply a device for measuring finger joint angles increases the complexity of the device and may affect the passive properties of the finger.

We have now developed an experimental protocol which uses a Polhemus sensor (3D location and orientation sensor) to identify the exact location and orientation of the finger tip relative to a fixed point on the hand. Using this method, the angles of the finger joints are calculated from the Polhemus sensor information, so that there is no need to attach a transducer directly to these joints. The protocols for use of this device will be described in the next few paragraphs. Using the reported sensor accuracy, we have determined the expected accuracy of the device given the protocols we established. We expect the device will be accurate to within 1 N-cm for moments measured at both joints, which is comparable to the accuracy of our current single joint device.

Assumptions for Mathematical Analysis

The following definitions and assumptions were necessary to develop the equations regarding the operation of this device:

1. The center of rotation for both the MP and PIP joints is assumed to be constant. The potential error due to a changing center of rotation can be identified experimentally.

2. There is a fixed point on the hand brace that is (Xoff, Yoff) from the MP center of rotation. This point is measured as part of the calibration of the device and never changes. It is assumed that this point always remains "fixed" to the metacarpal, and therefore to the MP joint center of rotation. Once Xoff and Yoff have been calculated, it is assumed that they remain constant throughout the remainder of the experiment.

3. The force/moment transducer is attached to the tip of the finger through a splint. The position of the transducer is known (Xt, Yt). It is assumed that this point is fixed relative to the splint, which is fixed relative to the finger tip, which is fixed relative to the PIP joint center of rotation.

4. The DIP joint is always immobilized with a splint and is never considered as a variable. The angle of the DIP joint is irrelevant as long as it doesn't change throughout the experiment.

Variable Definitions for Mathematical Analysis

1. X is defined as perpendicular to the plane of the palm, Y is defined as being parallel to the plane of the palm

2. +X is toward the thumb side (on a left hand), +Y is down the tip of the finger

3. The distance from the MP center of rotation (0,0) to the PIP center of rotation is Lp (proximal segment distance)

4. The distance from the PIP center of rotation to the position of the transducer (Xt,Yt) is Ld (distal segment distance)

5. There is an Mθ and a PIPθ which are defined as the angles between the two adjacent segments. 0 degrees is defined as full extension, positive angles indicate flexion, full flexion is typically 90 degrees.

6. There is a moment at the MP and PIP angles known as Mmp and Mpip.

Proposed Experimental Procedure for Passive Moment Device

The mathematical goal is to determine Mmp(Mθ, PIPθ) and Mpip(Mθ, PIPθ). Therefore, at any instant in time we must be able to calculate Mmp, Mpip, Mθ and PIPθ. The known variables will be (Xt,Yt), the forces and moments at the transducer (Ftx, Fty and MT), and one known reference point on the hand splint (initially defined as the coordinate frame origin). Throughout this analysis, we have assumed that we can directly measure the wrist angle and DIP angle using either a manual or electric goniometer. The angles of these two joints do not directly affect the accuracy of the moment calculations as long as their position remains fixed.

The general methods for making these measurements are:

1. Determine location of MP center of rotation and lengths of proximal and distal segments.

2. Determine movement and moment strategies so that each joint (MP, PIP) can be rotated while the other remains constant.

3. Calculate the moments about each joint as a function of the calculated angle of the joint.

The detailed protocols for each step are outlined below.

Step 1. Determine location of MP center of rotation and lengths of proximal and distal segments.

A dot (pen mark) is made on the lateral edge of the finger (so that it can be seen from above) just proximal to the PIP joint. A clear plexiglass plate with a thin black line on it is attached to the transducer . The position of the other end of the line is also recorded using the Polhemus sensor. The line is established so that it passes through the known point on the transducer at the tip of the finger. A second clear plexiglass plate is fixed to the hand splint and positioned so that the line passes directly over the dot on the finger. The lines on the two plexiglass pieces are made collinear. The PIP joint is rotated using the device so that the dot remains under the line on the plexiglass fixed to the hand (it doesn't have to stay there *during* the movement because this phase is only concerned with the endpoint). The location of the tip of the finger and the location of the second point on the distal line is recorded after the finger has been moved. There are a total of four pairs of points recorded. They are:

(X1,Y1) = "proximal point" for first position of finger (proximal is the point on the line that is away from the transducer point)
(X2,Y2) = transducer point for first position of the finger
(X3,Y3) = proximal point for second position of the finger
(X4,Y4) = transducer point for second position of the finger

From the four pairs of points, the center of rotation for the PIP joint can be calculated. Again, it is assumed that this center is constant between the two positions tested. The farther apart in angle the two

positions are, the lower the error. If necessary, the prediction error could be further reduced by repeating the measurement process at multiple angles and averaging.

The equations to calculate the PIP center of rotation are:

$$m12 = (Y2-Y1)/(X2-X1)$$
$$m34 = (Y4-Y3)/(X4-X3)$$

$$Xpip = (1/(m12-m34)) \bullet (m12 \bullet X1 - m34 \bullet X4 + Y4 - Y1)$$
$$Ypip = m12 \bullet (Xpip - X1) + Y1$$

$$Ld = \sqrt{(X4-Xpip)^2 + (Y4-Ypip)^2}$$

Where...

X1...Y4 = locations of position of plexiglass plate attached to transducer
m12, m34 = slopes of the line on the plexiglass plate
Xpip, Ypip = position of the center of rotation of the PIP joint
Ld = length of distal segment (PIP center of rotation to transducer point)

Next, the location of the MP center of rotation needs to be determined. The same procedure is used, only this time the PIP joint is kept constant and the MP joint is moved. A second dot is made on the finger just distal to the MP joint. Now the plexiglass piece attached to the transducer must be lined up with the two dots on the finger. The locations of the two points on the end of this piece are recorded. The finger is rotated to a new location, with the PIP joint kept straight so that the two dots remain under the line on the plexiglass. A new pair of points are recorded. Given the same definitions for points X1..Y4, the equations above are essentially identical...

$$m12 = (Y2-Y1)/(X2-X1)$$
$$m34 = (Y4-Y3)/(X4-X3)$$

$$Xmp = (1/(m12-m34) \bullet (m12 \bullet X1 - m34 \bullet X4 + Y4 - Y1)$$
$$Ymp = m12 \bullet (Xmp - X1) + Y1$$

$$Lp = \sqrt{((X4-Xmp)^2 + (Y4-Ymp)^2} - Ld$$

Given the point (Xmp, Ymp), it will be easier if those offsets are automatically subtracted from the measured Polhemus locations so that Xmp, Ymp becomes (0,0). The remaining equations assume that this has already been done.

Step 2. Determine movement and moment strategies so that each joint (MP, PIP) can be rotated while the other remains constant.

The movement strategies will be determined by trial and error because they are dependent not only on the joint kinematics, which are known, but also on the passive properties of each joint, which are not known. The device can move in the x and y directions and it can apply a torque about the tip of the finger about the z axis. The known values will be the position of the transducer and the applied forces and moments. An intelligent algorithm will be developed which will determine which way the device should move, or by how much the applied torque should change. Initially, this algorithm will be based on the expected passive moments, be we will evaluate other algorithms as well. After each incremental change, the joint angles are re-evaluated, and a new set of positions and moments is determined. This process is

repeated until the joint is moved through the entire range over which the measurements are to be made. If the passive moment remains constant (which we have verified from our earlier experiments), then repeating these movements and moments should generate the desired movement trajectory for the joint. The speed of the movement will affect the passive properties, but these changes are fairly predictable and consistent (once the joint has been warmed up), so it should be possible to determine the inputs necessary to move the joint through the same trajectory at faster speeds.

In order to record the joint angles, it is necessary to obtain an initial joint offset. The finger can be temporarily splinted straight. The transducer angle (θT) recorded from the Polhemus sensor is adjusted so that it corresponds directly to the angle of the distal finger segment relative to the metacarpal. This is the same as $\theta mp + \theta pip$.

The equations that allow the calculation of the joint angles given (Xt,Yt), θT and Ld are:

$$Xpip = Xt - Ld \bullet \sin\theta T$$
$$Xpip = Yt - Ld \bullet \cos\theta T$$

$$\theta mp = \tan^{-1}(Ypip/Xpip)$$
$$\theta pip = \theta T - \theta mp$$

Step 3. Calculate the moments about each joint as a function of the calculated angle of the joint.

The calibration of the apparatus is now complete, the joint centers of rotation are known and the joint trajectories have been established. It is now possible to perform a variety of movements of the finger while recording the passive moments. The device will be capable of performing these measurements automatically at various speeds.

The device measures and records the following information while the joints are being moved:

FTx = Force on transducer along the X axis
FTy = Force on transducer along the Y axis
MT = Moment on the transducer about the Z axis
Xt,Yt = Position of the transducer in space relative to MP center of rotation
θT = Angle of the transducer relative to y axis

First, at each point, the center of rotation for the PIP joint is calculated using the equations shown previously:

$$Xpip = Xt - Ld \bullet \sin\theta T$$
$$Xpip = Yt - Ld \bullet \cos\theta T$$

The joint moments are calculated as:

$$Mpip = -MT + (Xt - Xpip) \bullet FTy + (Yt - Ypip) \bullet FTx$$
$$Mmp = -Mpip - (Xpip - Xmp) \bullet FTy - (Ypip - Ymp) \bullet FTx$$

(Note: the point (Xmp,Ymp) should be (0,0))

Calculation of Expected Accuracy

It is possible to calculate the expected accuracy of this procedure if the accuracy of each of the measured variables can be determined. A Matlab routine was written to calculate the joint moments given repeated measures using values considered typical of the moments we have already measured from a single finger. The Matlab routine assumed that the variability of each value was distributed normally, with a standard deviation as shown below. The input variables were then allowed to vary randomly within their expected probability distribution, and the resulting joint moments were calculated. This procedure was repeated 1000 times, each time with a randomly chosen variation on the input variables. The average and standard deviations of the calculated joint moment values was determined from this data set. This provides a direct measure of the confounding effects of the variability in each measured parameter.

The expected accuracy of the measurements were as follows:

(X,Y) position accuracy = +/-0.8mm (along both axes). This is the stated accuracy of the Polhemus sensor in a static condition.

θT transducer angle accuracy = 0.15°. This is the stated accuracy of the Polhemus sensor in a static condition.

FT accuracy = +/- 0.1 Newton. This is consistent with similar transducers that we have developed in our own laboratory.

MT accuracy = +/- 0.5 N-cm. This is also consistent with similar transducers we have developed.

Ld = 15 cm or greater. This means that the transducer must be attached to the finger through a rod, making the effective length of the distal segment at least 15 cm.

Lp = 5 cm or greater

Mpip = 80 N-cm

Mmp = 130 N-cm

Joint angles at 45°

Estimated accuracy:
Ld accurate to +/- 0.015cm
Lp accurate to +/- 0.020cm

Mmp accurate to +/- 0.98 N-cm
Mpip accurate to +/- 1.12 N-cm

Summary

A design for a device capable of measuring passive moments of a two joint limb segment without splinting has been proposed. A mechanical analysis indicates that this design criteria can be achieved by applying the appropriate forces and moments onto the tip of the finger. An analysis of the expected device accuracy indicates that it should be able to calculate the MP moment to within +/- 0.98 N-cm and the PIP moment to within +/- 1.12 N-cm.

Plans for Next Quarter

During the next quarter, we will continue the analysis of the splintless passive moment device. Construction of a prototype device will begin to test the process using spring-loaded joints with known properties. The algorithm for producing the joint trajectories can then be tested.

1. b. BIOMECHANICAL MODELING: ANALYSIS AND IMPROVEMENT OF GRASP OUTPUT

Abstract

The ability to voluntarily extend the wrist is essential for providing functional use of the hand to persons with severe tetraplegia. Individuals with a C5 level spinal cord injury have severely weakened or paralyzed wrist extensors, limiting their ability to extend the wrist and preventing the development of a tenodesis grasp. In these individuals, it is common to transfer the distal tendon of the brachioradialis, an elbow flexor, to the distal tendon of the extensor carpi radialis brevis, one of the primary wrist extensors, to promote voluntary wrist extension. We are currently using a graphics-based computer model of the upper extremity to assess muscle function after a brachioradialis to extensor carpi radialis brevis tendon transfer (Br-ECRB).

Objective

The purpose of this project is to use the biomechanical model and the parameters measured for individual neuroprosthesis users to analyze and refine their neuroprosthetic grasp patterns.

Report of Progress

In the past quarter, we have simulated the tendon transfer using different tendon lengths to investigate the effects of surgical tensioning of the transfer on wrist function. Also, we have compared the moment-generating properties of the transfer in different wrist positions. Finally, we have incorporated a model of a weakened triceps muscle to simulate the elbow extension moment generated by neuroprosthesis users during electrical stimulation of the triceps or voluntarily after a posterior deltoid transfer.

The Effects of Surgical Tensioning on the Wrist Extension Moment Generated by the Br-ECRB Transfer

We developed the *initial model* of the Br-ECRB tendon transfer using the assumption that the surgery does not affect the force-generating capacity of the brachioradialis at the elbow joint (see previous progress report). When the wrist is in the neutral position (0° wrist flexion), the muscle fibers of the initial model operate on the ascending limb and plateau of the isometric force-length curve between full elbow extension (0° elbow flexion) and 130° flexion (Fig. 1.B.1A). As discussed in a previous progress report, this model indicates that the wrist extension moment generated by the transfer decreases substantially in flexed elbow positions, potentially limiting the ability to position the hand in tasks where the elbow is flexed. The initial model estimates a decrease in the wrist extension moment of 86% between 100° and 130° elbow flexion when the wrist is in the neutral position (Fig 1.B.2).

We developed a second model of the Br-ECRB tendon transfer (*tight transfer*) to produce a wrist extension moment that was less dependent on elbow position (Fig. 1.B.2). In the tight transfer, the tendon slack length of the initial model was shortened by 3 cm, causing the muscle fibers of the transfer to operate at longer lengths in the same elbow positions (Fig. 1.B.1B). The model indicates that the wrist extension moment generated by the tight transfer decreases by 27% between 100° and 130° elbow flexion, and the total moment varied by only 30% of maximum over the full range of elbow flexion. The model of the tight transfer also indicates that passive forces, generated by muscle fibers operating on the descending limb of the isometric force-length curve, are responsible for a substantial portion of the total wrist extension moment in extended elbow positions (Fig. 1.B.3). This differs from the transfer's function in the initial model of the surgery, where passive forces contribute very little to the wrist extension moment in full extension. The amount of passive wrist extension moment generated by the transfer is an important concern because if it is greater than the flexion moment generated at the wrist due to the weight of the hand, an individual with C5 level tetraplegia would be prevented from flexing his wrist using the effects of gravity.

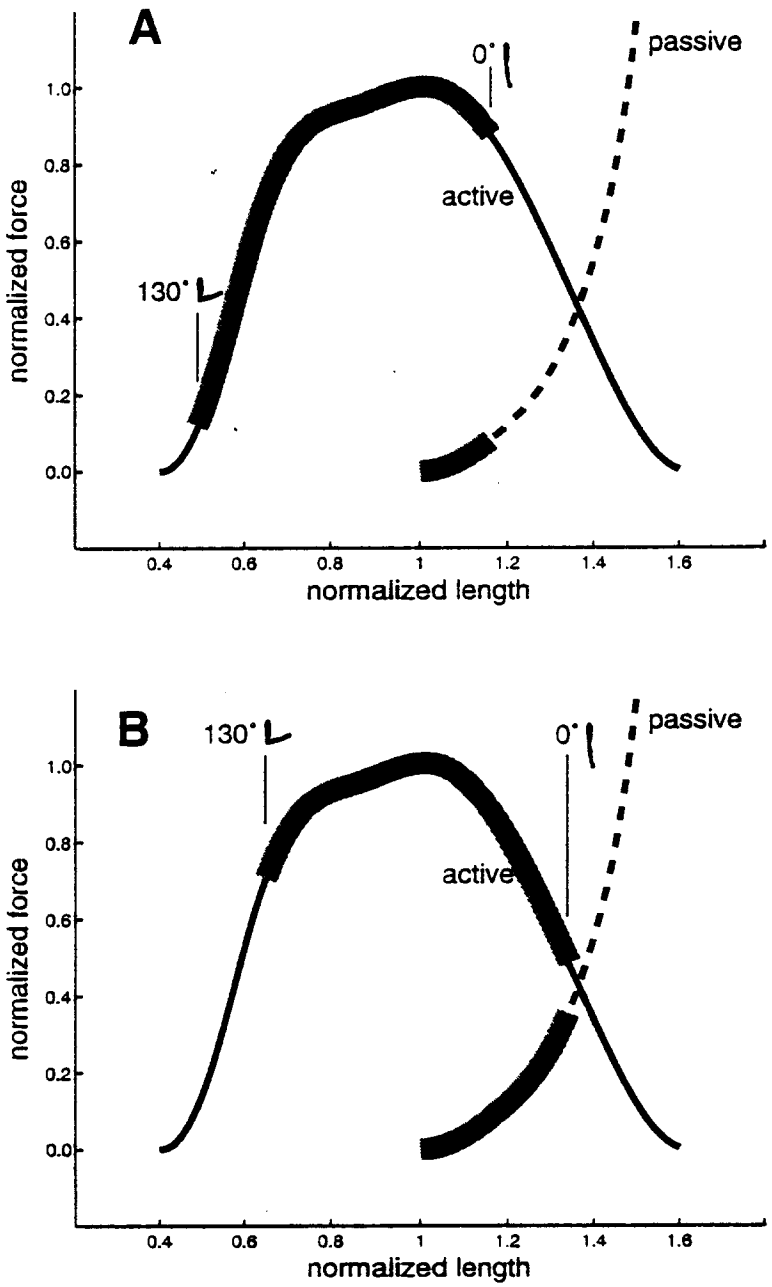

Figure 1.B.1. (A) Model estimates of the operating ranges of the transferred brachioradialis muscle fibers on the active and passive isometric force-length curves between full extension (0° elbow flexion) and 130° elbow flexion. The initial model operates on the plateau and ascending limb of the force-length curve. (B). Model estimates of the operating ranges of the transferred brachioradialis muscle fibers on the active and passive isometric force-length curves between full extension and 130° elbow flexion. The tight transfer operates primarily on the plateau and descending limb of the force-length curve.

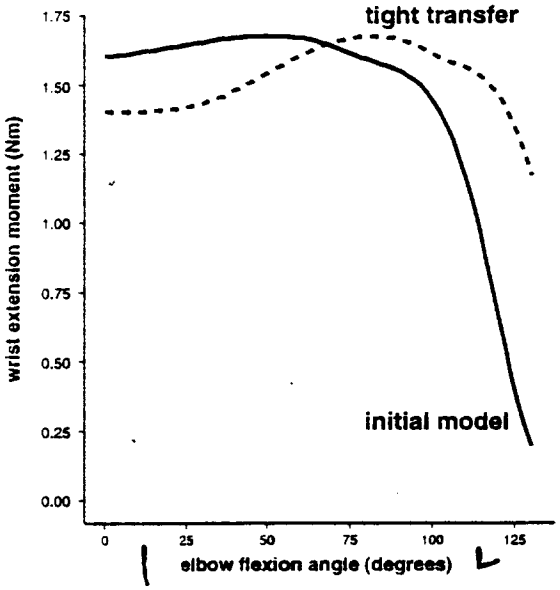

Figure 1.B.2. Estimate of the maximum isometric wrist extension moment generated by the Br-ECRB transfer as a function of elbow flexion angle using the initial model (solid line) and the model of the tight transfer (dashed line). The wrist is in the neutral position (0° wrist flexion) in both models. The wrist extension moment of the initial model decreases substantially in flexed elbow positions, while the model estimate of the moment generated by the tight transfer varies less over the full range of elbow flexion.

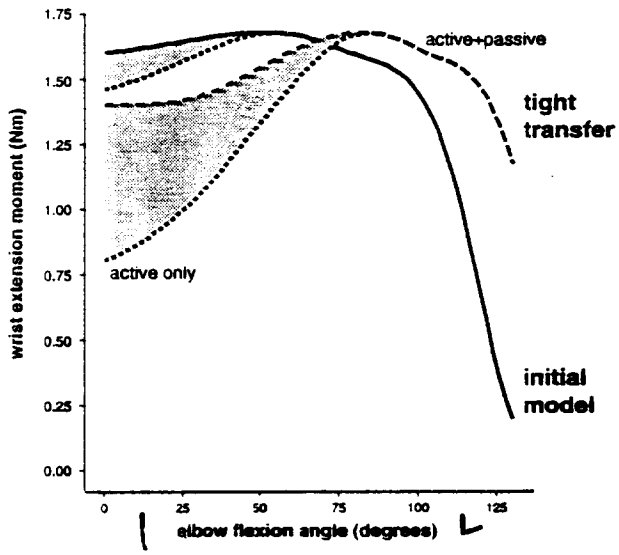

Figure 1.B.3. Estimates of total wrist extension moment generated by the Br-ECRB transfer as a function of elbow flexion angle using the initial model (solid line) and the model of the tight transfer (large dashed line), the wrist extension moment actively generated by the two transfers (small dashed lines), and the wrist extension moment generated passively by the two transfers (shaded gray areas). The wrist is in the neutral position (0° wrist flexion) in both models. For the initial model, the contribution of passive forces to the total wrist extension moment is minimal. However, the passive moment generated by the tight transfer is responsible for a substantial portion of the total wrist extension moment in extended elbow positions.

The Effects of Wrist Position on the Wrist Extension Moment Generated by the Br-ECRB Transfer

The moment-generating properties of the transfer at the wrist change with wrist position because the muscle fibers of the transferred brachioradialis shorten when the wrist is extended and lengthen when the wrist is flexed, shifting the fiber operating range on the isometric force-length curve. Also, the wrist extension moment arm of the transfer decreases in flexed wrist postures (Fig. 1.B.4). In both models of the transfer, when the wrist is in the extended position, the operating range of the transferred muscle includes a greater portion of the ascending limb compared to the operating range when the wrist is in the neutral position. This results in a substantial decrease in moment-generating capacity in flexed elbow positions (Fig. 1.B.5). In fact, with the wrist extended and the elbow fully flexed, the muscle fibers of the initial model are too short to actively generate force, and the moment-generating capacity of the transfer in this arm posture is zero. In the flexed wrist position, the lengthened fibers of the transferred brachioradialis use less of the ascending limb, and the moment generated in flexed elbow postures is maintained at a higher level. However, because wrist flexion decreases the wrist extension moment arm of the transfer, the extension moment the transfer is capable of generating is compromised in all but the most flexed elbow postures (Fig. 1.B.5).

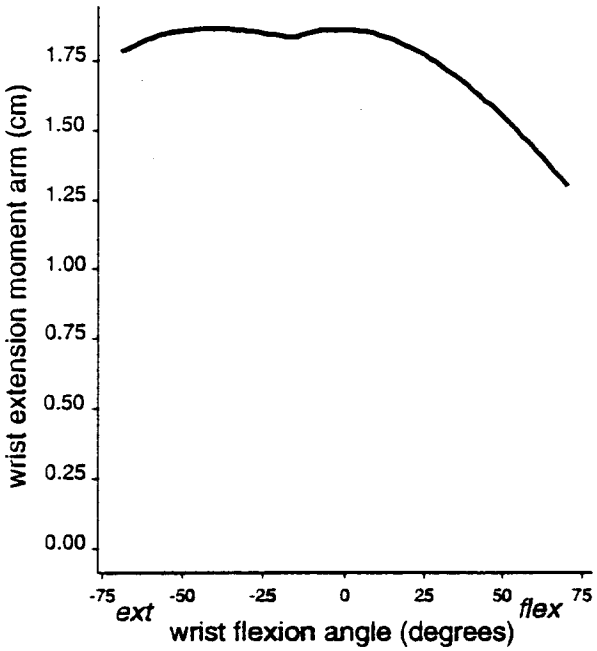

Figure 1.B.4. Wrist extension moment arm of the Br-ECRB transfer. The magnitude of the moment arm decreases in flexed wrist positions.

The goal of the tight transfer was to produce a wrist extension moment that was less dependent on elbow position than the initial model. However, the broad operating range of the brachioradialis as a function of elbow flexion angle combined with the additional excursion imposed on the muscle during wrist movement make it difficult to avoid the ascending limb over the full range of elbow and wrist positions. Thus, it seems impossible to completely eliminate the dependence of wrist extension strength on elbow position after a Br-ECRB transfer. In addition, regardless of surgical tensioning, the model indicates that wrist extension strength is weakest in flexed wrist positions due to the smaller wrist extension moment arm in this position.

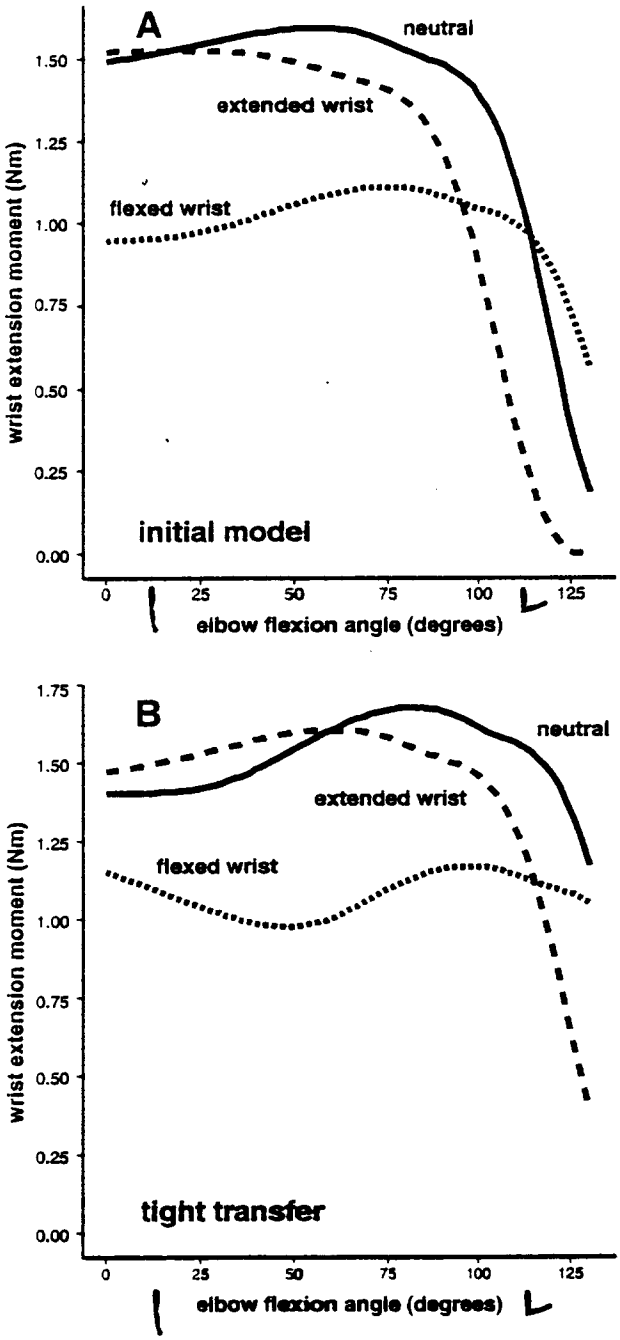

Figure 1.B.5. (A) Estimates of total wrist extension moment generated by the initial model of the Br-ECRB transfer as a function of elbow flexion angle in different wrist postures. With the wrist extended, the muscle fibers operate at shorter fiber lengths compared to the neutral wrist position, decreasing the isometric moment-generating capacity of the muscle. The moment-generating capacity of the transfer is compromised when the wrist is flexed due to the smaller wrist extension moment arm in this position. (B) Estimates of total wrist extension moment generated by the tight transfer as a function of elbow flexion angle in different wrist postures. In the neutral wrist position, the moment generated by the transfer is maintained in flexed elbow positions. However, the wrist extension moment generated by the transfer is still highly dependent on elbow position when the wrist is extended. Like the initial model, wrist flexion compromises the wrist extension strength of the tight transfer.

Muscle Function at the Elbow Joint

After transfer, when the brachioradialis is activated to generate wrist extension, it also generates an elbow flexion moment. The model indicates that the magnitude of the moment generated by the transfer varies as a function of both elbow and wrist positions. In general, the magnitude of the elbow flexion moment generated by the transfer is substantially greater than the elbow flexion moment the ECRB is normally capable of generating (Fig. 1.B.6). Thus, the Br-ECRB transfer amplifies the link between elbow flexion and wrist extension.

The action of the Br-ECRB transfer at the elbow joint must be balanced if the arm position is to be maintained during a wrist extension task. However, triceps function is absent in individuals with a C5 level spinal cord injury. In most individuals, some degree of voluntary elbow extension is provided via (i) a tendon transfer which attaches the posterior deltoid to the insertion of the triceps and/or (ii) functional electrical stimulation of the triceps. As an initial simulation of the elbow extension moment generated under these conditions, we developed a model of a weakened triceps by combining the force-generating capacity of the lateral and medial heads of the triceps (rather than combining the force-generating capacity of all three heads of the triceps). The current model indicates that the magnitude of the elbow extension moment generated by the weakened triceps is comparable to the magnitude of the elbow flexion moment generated by the transfer in elbow positions ranging from 75° flexion to 120° flexion. Thus, it is possible that the elbow flexion moment generated by the transferred brachioradialis is greater than the elbow extension moment provided by a weak elbow extensor in specific elbow positions. This could further limit wrist function, because an individual would be unable to fully activate the brachioradialis in these elbow postures. Consequently, the muscle would generate a smaller force and wrist extension moment.

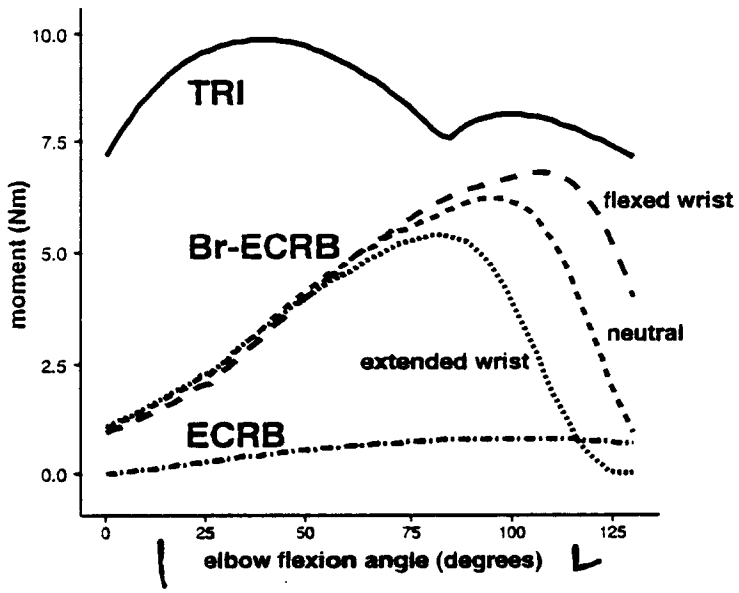

Figure 1.B.6. Estimated magnitude of the elbow flexion moments generated by the ECRB and the initial model of the Br-ECRB transfer, and the elbow extension moment generated by a weakened triceps. In most arm postures, the moment-generating capacity of the transfer at the elbow is substantially greater than the elbow flexion moment the ECRB is normally capable of generating. In addition, between 75° and 120° elbow flexion, the elbow flexion moment generated by the transfer approaches the moment-generating capacity of a weak triceps.

Plans for Next Quarter

In the next quarter, we plan to further investigate the effects of surgical tensioning of the Br-ECRB transfer on wrist function. We plan to compare the range of motion at the wrist provided by the initial

model and the tight transfer. We also plan to evaluate how wrist range of motion is influenced by elbow position and elbow extension strength.

2. CONTROL OF UPPER EXTREMITY FUNCTION

Our goal in the five projects in this section is to either assess the utility of or test the feasibility of enhancements to the control strategies and algorithms used presently in the CWRU hand neuroprosthesis. Specifically, we will: (1) determine whether a portable system providing sensory feedback and closed-loop control, albeit with awkward sensors, is viable and beneficial outside of the laboratory, (2) determine whether sensory feedback of grasp force or finger span benefits performance in the presence of natural visual cues, (of particular interest will be the ability of subjects to control their grasp output in the presence of trial-to-trial variations normally associated with grasping objects, and in the presence of longer-term variations such as fatigue), (3) demonstrate the viability and utility of improved command-control algorithms designed to take advantage of forthcoming availability of afferent, cortical or electromyographic signals, (4) demonstrate the feasibility of bimanual neuroprostheses, and (5) integrate the control of wrist position with hand grasp.

2. a. HOME EVALUATION OF CLOSED-LOOP CONTROL AND SENSORY FEEDBACK

Abstract

The purpose of this project is to deploy an existing portable hand grasp neuroprosthesis capable of providing closed-loop control and sensory feedback outside of the laboratory. We are exploring the possibility of constructing a stand-alone, single-channel grasp force sensory feedback system for implementation outside of the laboratory, independent of any support devices.

Purpose

The purpose of this project is to deploy an existing portable hand grasp neuroprosthesis capable of providing closed-loop control and sensory feedback outside of the laboratory. The device is an augmented version of the CWRU hand neuroprosthesis, and was developed and fabricated in the previous contract period. The device utilizes joint angle and force sensors mounted on a glove to provide sensory information, and requires daily support from a field engineer to don and tune. The portable feedback system is not intended as a long term clinical device. Our goal, rather, is to evaluate whether the additional functions provided by this system benefit hand grasp outside of the laboratory, albeit with poor cosmesis and high demands for field support.

Report of Progress

As reported last quarter, we are modifying the implementation of the portable feedback system in order to gain access to a larger population of patients. It seems most reasonable to construct a single-channel grasp force feedback device that is capable of being donned and used independently of the neuroprosthesis. Such a device would consist of the thumb-mounted sensor described previously, and a processing and stimulation unit with attached electrode that would be strapped to a user's upper arm. We have approached two manufacturers of neuroprosthetic devices (NeuroControl Corp. and NeuroMotion Inc.) but neither were able to provide or develop such hardware. Therefore, we are now investigating modifications of the stimulators built for the existing portable feedback system for the revised application.

Plans for Next Quarter

We will attempt to modify the circuitry of the existing surface stimulation channels to build a small, battery powered unit suitable for wear on the arm. We anticipate that all controls used for setting the force-to-stimulus map will be analog and directly user (or attendant) settable. If possible, we will construct a prototype unit for evaluation. We will also continue our search for a commercial stimulator that could be used for the purpose.

2. b. INNOVATIVE METHODS OF CONTROL AND SENSORY FEEDBACK

2. b. i. ASSESSMENT OF SENSORY FEEDBACK IN THE PRESENCE OF VISION

Abstract

The purpose of this project is to develop a method for including realistic visual information while presenting other feedback information simultaneously, and to assess the impact of feedback on grasp performance in the presence of such visual information. In this quarter, we have implemented a robust, model referenced adaptive controller that will allow us to accommodate both the nonlinearities in recruitment functions as well as the dynamics of the neuroprosthesis system (including delays) so that we can collect optimal, smooth video clips for use in the video-based simulation system.

Purpose

The purpose of this project is to develop a method for including realistic visual information while presenting other feedback information simultaneously, and to assess the impact of feedback on grasp performance. Vision may supply enough sensory information to obviate the need for supplemental proprioceptive information via electrocutaneous stimulation. Therefore, it is essential to quantify the relative contributions of both sources of information.

Report of Progress

As discussed in previous reports, realistic visual feedback via digitized video requires a smooth playback of the pre-recorded video clips. Smoothness requires that the neuroprosthesis output change at a constant rate to ensure that there are no abrupt changes between video frames. It is necessary then to modulate the rate change of the input command in order to accommodate for irregularities in the recruitment curves of neuroprosthesis users.

In the previous report, we described a "line integral algorithm" for adaptively modulating the command signal to the neuroprosthesis to yield video clips with frames spaced equally along the static recruitment function (i.e., the functions relating output force to input command). The algorithm worked well in some cases, but not all. The algorithm could, in principle, compensate for any irregularities in the recruitment function (including non-monotonicities) as long as there were no delays in the system. However, the line-integral algorithm was incapable of compensating for system dynamics. (By "system," we include all components between the input command signal and the output force: neuroprosthesis, musculature, hand, object, and sensor.) In particular, the algorithm could not generate the acausal command signals required to compensate for system delays since it had no ability to predict future outputs that would result from current and past inputs. It is not sufficient, then, to use the line-integral algorithm (or other similar method) to simply "invert" the recruitment function for a given user. Instead, we propose modeling the complete system as a lumped single-input (command), single-output (force) system using a Hammerstein structure which includes a static non-linearity (recruitment function) followed by a linear dynamic system (including a delay) [1]. We are in the process of creating the model using data collected recently from one neuroprosthesis user. Band-limited noise (5th order, 100 Hz cutoff) was input as the command signal to the neuroprosthesis, and the resulting forces were measured. The system model will be identified using Matlab routines developed in-house.

The model identified for one neuroprosthesis user at particular time will not represent all other users at all times. Recruitment properties change for a single user over time due to movement, length-dependence, and fatigue [2,3], and are certainly different among different users. A single model will suffice, however, if it is incorporated into a model referenced adaptive control (MRAC) algorithm [4], as sketched in Figure 2.b.1. First, we specify a desired output trajectory $y(k)$, where k is the current time step In this case, we want the output force to increase at a constant rate over time so that it changes by a fixed amount between video frames. The desired output and the reference model are then used to calculate the nominal input $u(k)$ that would yield $y(k)$ *if* the real system behaved exactly like the model. $u(k)$ is input into the controller, which in turn generates the input $u^*(k)$ to the actual plant (the neuroprosthesis, etc.). The resulting output $y^*(k)$, the reference model output $y(k+d)$, and the controller output $u^*(k)$ are all used to adjust the controller parameters. Note that the reference model output incorporates the estimated delay d in the system. The adjustment algorithm shifts the model output by an amount $-d$ prior to comparing it to the

actual output $y^*(k)$, as shown in the block diagram. The controller parameters are adjusted to optimize the tracking between the nominal and actual outputs, without making adjustments to the reference model. We have completed the software needed to implement the MRAC in the video collection software. The performance of the algorithm has been tested using known but mismatched first-order systems for the plant and the model, and a ramp input signal for $u(k)$. As expected, the output error rapidly converged to zero. Actual data collection will be pursued throughout the next quarter.

Plans for Next Quarter

The MRAC algorithm is complete and we have scheduled neuroprosthesis users for data collection sessions. The emphasis in the next quarter will be on assembling a large number of video clips for use both in the evaluation of sensory feedback and for assessing control methods.

References

[1] Durfee WK, MacLean KE (1989) Methods for estimating isometric recruitment curves of electrically stimulated muscle. IEEE Trans BME 36(7)::654-667

[2] Crago PE, Peckham PH, Thrope GB (1980) Modulation of muscle force by recruitment during intramuscular stimulation. IEEE Trans BME 27: 679-684.

[3] Hines AE, Owens NE, Crago PE (1992) Assessment of input-output properties and control of neuroprosthetic hand grasp. IEEE Trans BME 39: 610-623.

[4] Landau I, Lozano R (1981) Unification of discrete time explicit model reference adaptive control designs. Automatica 17: 593-611.

2. b. ii. INNOVATIVE METHODS OF COMMAND CONTROL

Abstract

During this quarter we began evaluation of command control algorithms using a computer-based video simulator. Subjects used shoulder position to control a video image of neural prosthetic hand grasp. The users had to adjust the grasp force to within a specified window and hold it there for 5 s. Results indicate that performance improved as the size of the grasp force window was increased.

Purpose

The purpose of this project is to improve the function of the upper extremity hand grasp neuroprosthesis by improving user command control. We are specifically interested in designing algorithms that can take advantage of promising developments in (and forthcoming availability of) alternative command signal sources such as EMG, and afferent and cortical recordings. The specific objectives are to identify and evaluate alternative sources of logical command control signals, to develop new hand grasp command control algorithms, to evaluate the performance of new command control sources and algorithms with a computer-based video simulator, and to evaluate neuroprosthesis user performance with the most promising hand grasp controllers and command control sources.

Report of Progress

During this quarter we began using the computer-based video simulator (see C.2.b.i) to evaluate algorithms for command control of neuroprosthetic hand grasp. In this virtual evaluation, subjects control the opening and closing of a video image of neural prosthetic hand grasp. In these initial studies we began collecting baseline command control performance data with the standard shoulder position proportional control.

METHODS

In these evaluations, subjects used a joystick mounted on the shoulder to control opening and closing of the virtual grasp. The middle 50% of the subjects' shoulder elevation range of motion was mapped into 0-100% command, and used to control which frame of the video was displayed.

The virtual task used for evaluation of command control was that same as that designed for evaluation of the portable feedback system. The subject had to create a command signal that resulted in a grasp force

within a pre-defined window ("acquire") and maintain the command within the window for a defined time ("hold"). A successful acquisition meant that the grasp force was within the window at some point during the acquire phase. A successful hold meant that the grasp force was maintained within the window for the hold period, and a successful "task" meant that both acquire and hold were successful. The subjects were allowed five practice trials at the beginning of each block in which they were provided visual feedback of the grasp force target window and the actual grasp force. During testing, subjects were only provided with the visual image of the virtual hand. Subjects used visual cues from the video as well as shoulder proprioception to make appropriate commands. In these trials the acquire time and hold time were each fixed at 5 s, the target force was fixed, and the size of the grasp force window was varied. Each subject completed 20 trials at each of 5 grasp force window sizes. In these initial experiments, the same video clip was used for all trials. Thus, results may reflect use of visual cues which would not be present in actual use of a hand grasp neural prosthesis.

RESULTS

The success rate for the acquisition phase and the complete acquire+hold task are shown as a function of the grasp force window size in figure C.2.b.ii.1 for 3 subjects. Subjects 1 and 3 showed a clear and apparently linear relationship between the success at the acquire and hold task and the size of the grasp force window. Subject 2 exhibited no clear relationship between the success rate and the size of the window, but the two blocks at the smallest window size (5 %) had the lowest rate of success. Subject 1 also showed a clear increase in success at the acquire phase of the task when comparing the two smallest window sizes (5 %, 10 %) to the larger window sizes, while subjects 2 and 3 exhibited no clear relationship between success in the acquire phase and the grasp force window size. These data indicate that the performance in the hold phase of the task improved as the grasp force window size was increased.

One confounding effect which might be present in these results is learning. Subjects might identify a cue in the video clip (recall that the same video clip was used for all trials) which they can then use to attain the correct command, irrespective of the window size. To examine the effect of experience, the success rate was plotted as a function of the block number (fig. C.2.b.ii.2). None of the subjects exhibited a clear trend in success rate across the blocks. In subject 2, in which the 5 % window size was repeated in blocks 4 and 5, the performance actually decreased between these blocks. These data suggest that, even with the same clip repeated in every trial, that the results shown in fig. C.2.b.ii.1 cannot be attributed to learning.

Plans for Next Quarter

In the next quarter we will continue command control algorithm evaluation using the video simulator.

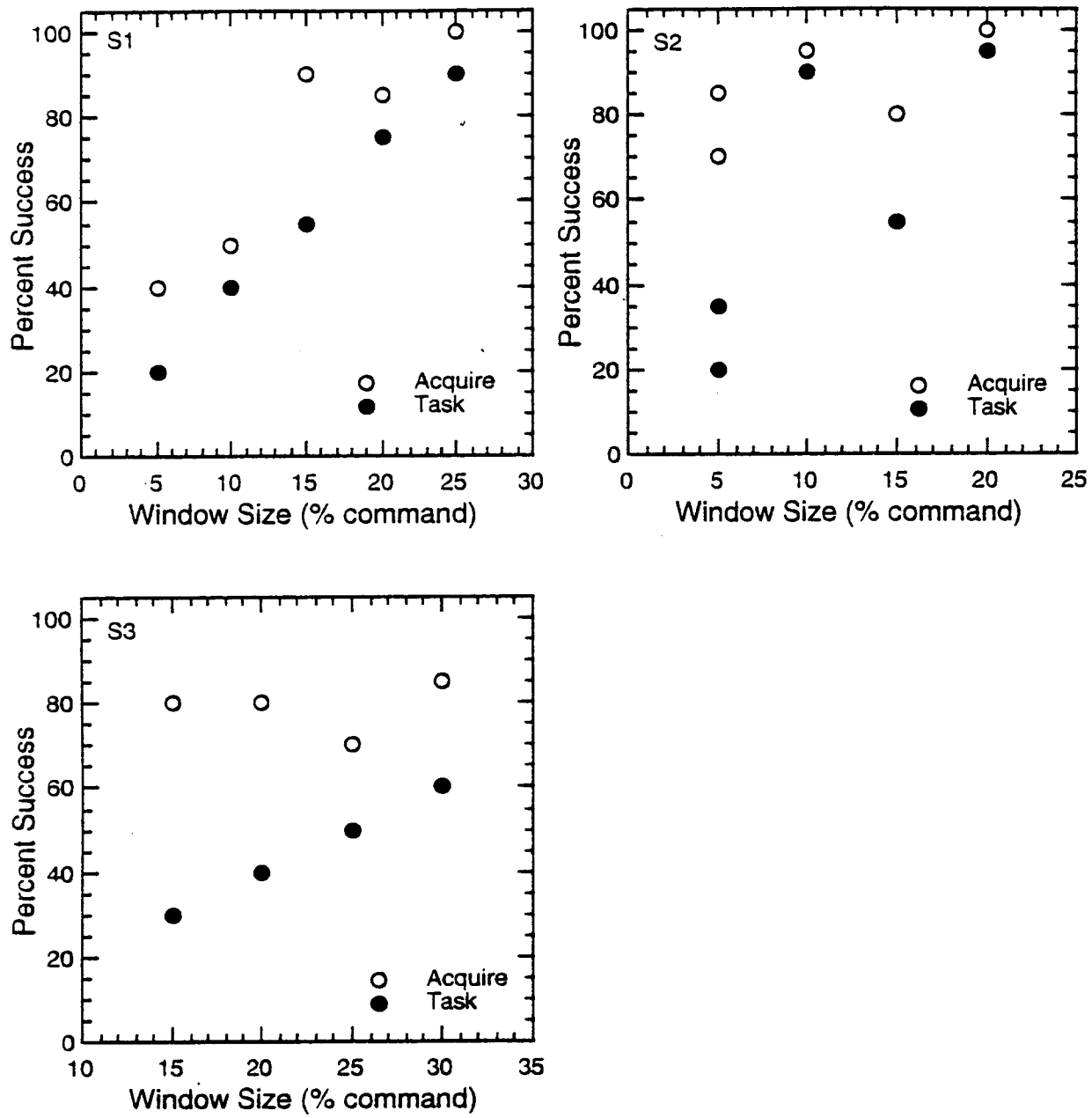

Figure C.2.b.ii.1: The success rate for the acquire phase and the complete acquire and hold (task) as a function of grasp force window size for 3 subjects (S1, S2, S3). Each point represents the success rate across 20 trials at the same target force and grasp force window size.

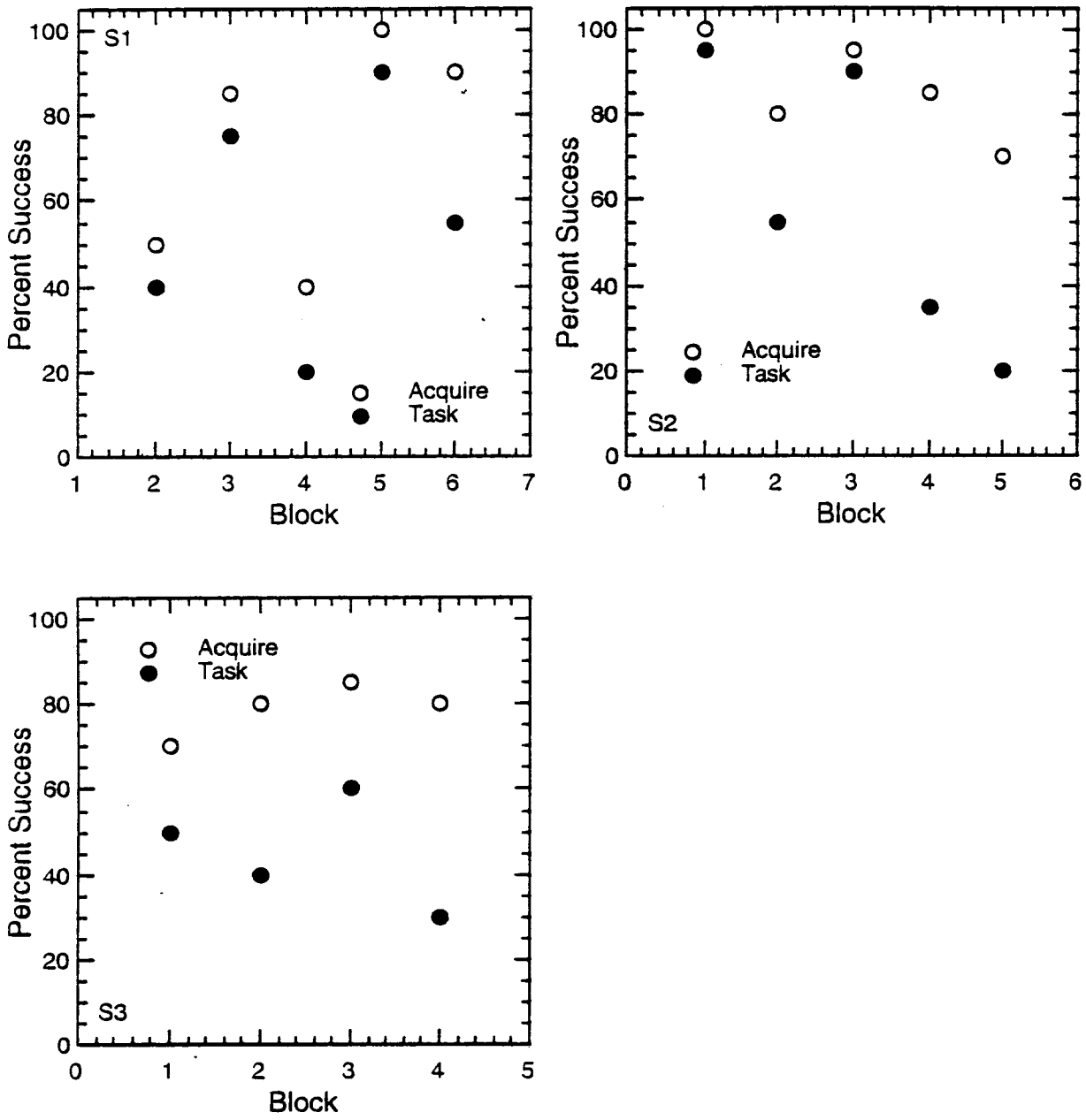

Figure C.2.b.ii.2: The success rate for the acquire phase and the complete acquire and hold (task) as a function of the block number (i.e., time) for 3 subjects (S1, S2, S3). Each point represents the success rate across 20 trials at the same target force and grasp force window size.

2. b. iii. INCREASING WORKSPACE AND REPERTOIRE WITH BIMANUAL HAND GRASP

Abstract

Two possible command-control algorithms for a hand neuroprosthesis using the EEG signal have been identified. These algorithms are based on analysis of the data provided by Dr. Jonathan Wolpaw (Wadsworth Center, Albany, NY) on five able bodied subjects. These two algorithms were outlined in the previous progress report, along with preliminary data analysis from two subjects. Also, two subjects have completed the initial screening process and have started training on moving a cursor on the computer screen using the EEG signal. An initial analysis from the screening process is also presented.

Purpose

The objective of this study is to extend the functional capabilities of the person who has sustained spinal cord injury and has tetraplegia at the C5 and C6 level by providing the ability to grasp and release with both hands. As an important functional complement, we will also provide improved finger extension in one or both hands by implantation and stimulation of the intrinsic finger muscles. Bimanual grasp is expected to provide these individuals with the ability to perform over a greater working volume, to perform more tasks more efficiently than they can with a single neuroprosthesis, and to perform tasks they cannot do at all unimanually.

Report of progress

In this quarter, analysis of the data provided by Dr. Wolpaw was completed and two command-control strategies for using the EEG signal to operate the neuroprosthesis were identified. As discussed in QPR # 7, the first method would be to use the EEG signal in the same manner as a switch or binary signal. For example, movement of the cursor up and the high voltages it generates would be considered a '0' and the downward cursor movement with its lower voltages would be considered a '1'. The EEG signal could then be used to control the operational state of the neuroprosthesis (on/off/lock) or to operate a gated ramp to control hand opening and closing. While this type of information has been used in the past to operate a neuroprosthesis, it is not the ideal method of control because it has inherent time delays. The other method in which the EEG signal can be used is that the downward cursor movement, with its larger voltage range (approximately 45 units) might be used to generate a proportional signal to control hand opening and closing, while the upward cursor movement, with its smaller but significant voltage change, can be used to operate system state (on/off) or just as a locking signal.

Studies to this date have focused exclusively on the second (preferred) method of using the EEG signal to operate the neuroprosthesis. Setting a high threshold level to trigger a state change and determining a linear equation to convert the downward cursor movement into a proportional control signal, it has been determined that the threshold levels are constant within a subject over multiple trials with a deviation of approximately +/- 0.5 mV but not across subjects (as would be expected), and that the slope for the linear equation is also constant, with a +/- 0 deviation. The values for the thresholds and the slopes of the linear equations for each subject are given in Table 2.B.iii.1.

With the establishment of two possible means by which the EEG signal can be used to operate a neuroprosthesis, we have started screening potential subjects for our own EEG studies. To date, three subjects (two able bodied and one neuroprosthesis user) have undergone the initial screening session. Data from one subject (the neuroprosthesis user) was discarded due to noise problems associated with the signal processing board and the analog/digital input boards. This problem has been corrected, and did not affect the data from the other subjects.

Subject (# of trials)	Threshold (+/- S.D)	Slope
A (n=2)	-17.8 (0.35)	10
B (n=3)	28.7 (0.57)	10
C (n=1)	-11.0	10
D (n=2)	-8.8 (0.35)	20
E (n=4)	11.3 (0.57)	20

Table 2.B.iii.1 : Threshold and slope values for command-control in all five subjects

The subjects underwent three separate protocols during the screening session with each protocol used to define areas of the cortex which were active with hand, elbow and shoulder movement. The protocols were also used to define cortical areas which were active with the visualization of these movements. The use of three separate protocols in the initial screening session varies significantly from the studies conducted by Dr. Wolpaw. Dr. Wolpaw and his colleagues only focused on hand movement, and used the signals generated by cortical areas active during this type of movement for cursor control. The use of the three protocols which examine elbow and shoulder movement in addition to hand movement will identify areas of cortical activity in the able bodied subjects during the execution of these movements, and then determine how the C5/C6 level spinal cord injury affects this. We expect a significant degree of cortical reorganization to occur with the spinal cord injury, which has definite implications in using the cortical activity of the hand areas to control cursor function. By performing a more extensive screening session, it will be possible to determine if there is still a cortical response to hand movement in persons with a C5/C6 level injury , if this area has been entirely remapped by elbow and shoulder movement, or if there exists some hybridization of the two extremes.

Initial results from the two able bodied subject are shown in Table 2.B.iii.2. The first column lists the location of the cortical activity (based on the modified 10-20 system), and the second column gives the frequency band in which activity is occurring with movement or visualization of movement. Only the hand and elbow movements are shown. The data from the second subject with shoulder movement is not complete at this time. The table demonstrates that activity with hand movement and the visualization of movement is the same for both subjects. Elbow movement and its visualization, however, shows differences between the two subjects. This is to be expected since there do exist differences between individuals as far as how the body and its extremities are mapped over the motor cortex. However, the general areas of cortical activity with elbow movement and the visualization of its movement are consistent with the somatotopic representation which is expected to be present in the able bodied cortex.

An attempt was also made to examine the pre-frontal cortex and examine cortical activity with movement and the visualization of movement. There is activity in the prefrontal area with movement and its visualization, as would be expected, but no clear patterns of cortical activity are noticeable from such a limited data base. It is hoped that with more subjects some insight may also be gained into the functioning of the pre-motor areas that may also be used for EEG based control of the neuroprosthesis.

Plans for Next Quarter

During the next quarter, we will recruit more able bodied subjects and neuroprosthesis users for this study. The screening data from these subjects will provide us with a greater data base to allow for a definition of the difference between the able bodied motor cortex and one which has been changed due to spinal cord injury. This information will also allow us to select appropriate sites to record the EEG signal from in the neuroprosthesis users, and which could possibly allow for control of the neuroprosthesis without interference from movement of the elbow and shoulder. The subjects will also be trained in the operation of cursor movement with the EEG signal, which will then allow us to better define the characteristics of the EEG signal, and provide us with a potential group of users for the EEG-based controller.

	Cortical Areas Active	Frequency
Subject 1 - hand movement	C3, C4	9, 12 Hz
Subject 2 - hand movement	C3, C4	9, 12 Hz
Subject 1 - elbow movement	C2	24, 27 Hz
Subject 2 - elbow movement	Cz	21, 24 Hz
Subject 1 - visual (hand)	C3, C4 C1, C2	9,12 Hz 21, 24 Hz
Subject 2 - visual (hand)	C3 C1, C2	9,12 Hz 21, 24 Hz
Subject 1 - visual (elbow)	C2	24, 27 Hz
Subject 2 - visual (elbow)	C5, C3, C4, C6 C1	9,12 Hz 21, 24 Hz

Table 2.B.iii.2 : List of active cortical areas and the frequencies for both subjects with hand and elbow movement/ visualization of movement.

2. b. iv CONTROL OF HAND AND WRIST

Abstract

We have nearly completed a manuscript describing our previous work on coordinated feedforward control of wrist angle and hand grasp. We have also initiated a project to examine the biomechanics of the extensor carpi ulnaris to extensor carpi radialis brevis transfer, which is an important component of restoring wrist extension.

Purpose

The goal of this project is to design control systems to restore independent voluntary control of wrist position and grasp force in C5 and weak C6 tetraplegic individuals. The proposed method of wrist command control is a model of how control might be achieved at other joints in the upper extremity as well. A weak but voluntarily controlled muscle (a wrist extensor in this case) will provide a command signal to control a stimulated paralyzed synergist, thus effectively amplifying the joint torque generated by the voluntarily controlled muscle. We will design control systems to compensate for interactions between wrist and hand control. These are important control issues for restoring proximal function, where there are interactions between stimulated and voluntarily controlled muscles, and multiple joints must be controlled with multijoint muscles.

Report of progress

The manuscript describing our simulation and experimental demonstration of coordinated integrated control of hand grasp and wrist angle is nearly completed. We expect to submit it for review in the next quarter.

The ECU to ECRB transfer provides an important source of extension moment to restore wrist extension in C5 and weak C6 tetrapelgia. Thus, it is important to understand its performance so that the effects of transfer can be predicted prior to surgery, and so that the transfer procedure can be optimized.

The simplest biomechanical model of tendon transfer assumes that the muscle retains its length-tension property, but acts through the moment arm of its target tendon. We are testing the appropriateness of this model by measuring the moment-angle and moment arm-angle relationships of the extensor carpi ulnaris

before and after transfer. Both wrist moment measurements and the MRI moment arm estimation technique described in Section 1, play an important role in this project.

After the ECU tendon is transferred to the tendon of the ECRB, the extension moment *vs.* wrist angle relationship will be the force generated by ECU acting via the moment arm of the ECRB. We hypothesize that the moment-angle relationship after transfer can be calculated from the force-length property of the ECU measured before transfer, and the moment arm *vs.* wrist angle relationship for ECRB also measured before transfer. The hypothesis is based on two assumptions: 1) the length-tension property of the ECU is not altered by the tendon transfer surgery, and 2) the transfer does not alter the moment arm of the ECRB.

We have designed a new wrist moment transducer, based on the same design principles of our finger moment and elbow moment transducers reported previously [Kilgore et al. 1998]. Mechanical drawings have been sent to a machinist for production. This transducer will improve over our previous method of measuring wrist moments with the JR3 multiaxis force/moment transducer, and will offer distinct advantages. The primary advantage is that the device will be fixed to the forearm proximal to the wrist, and span the wrist. This will eliminate the need to fix both the forearm and the sensor to the same mechanical reference point, and should reduce the influence of body movements on the moment measurements. The new device will also allow changes in wrist angle in either the flexion/extension or radial/ulnar deviation axes without having to realign the transducer. Finally, the moment measurements will not depend on estimates of center of rotation of the wrist.

The ECU length-tension property will be calculated from the moment-angle relationship measured during stimulation, and the estimated moment arm-angle relationship obtained from MRI. The expected moment-angle relationship after transfer to the ECRB tendon will be calculated from the calculated ECU length-tension property and the moment arm-angle relationship of the ECRB tendon also estimated by MRI. The expected moment-angle relationship will be compared to the actual moment-angle relationship measured by electrical stimulation after transfer. We are currently simulating this modeling procedure to optimize the number of measurements to be made and to examine the potential limitations of the technique.

Plans for next quarter

The parts for the wrist moment transducer should be received from the machinist, and we expect to assemble and calibrate the device. We also expect to complete the second wrist control manuscript and submit it for publication.

References

Kilgore, K.L., Lauer, R.J., and Peckham, P.H., A transducer for the measurement of finger joint moments, IEEE Trans. Rehab. Eng., in press, 1998.